Igneous mineralogy at Bradbury Rise: The first ChemCam campaign at Gale crater

V. Sautter,[1] C. Fabre,[2] O. Forni,[3] M. J. Toplis,[3] A. Cousin,[4] A. M. Ollila,[5] P. Y. Meslin,[3] S. Maurice,[3] R. C. Wiens,[4] D. Baratoux,[3] N. Mangold,[6] S. Le Mouélic,[6] O. Gasnault,[3] G. Berger,[3] J. Lasue,[3] R. A. Anderson,[7] E. Lewin,[8] M. Schmidt,[9] D. Dyar,[10] B. L. Ehlmann,[11] J. Bridges,[12] B. Clark,[13] and P. Pinet[3]

[1] Textural and compositional analyses using Chemistry Camera (ChemCam) remote microimager and laser-induced breakdown spectroscopy (LIBS) have been performed on five float rocks and coarse gravels along the first 100 m of the Curiosity traverse at Bradbury Rise. ChemCam, the first LIBS instrument sent to another planet, offers the opportunity to assess mineralogic diversity at grain-size scales (~ 100 μm) and, from this, lithologic diversity. Depth profiling indicates that targets are relatively free of surface coatings. One type of igneous rock is volcanic and includes both aphanitic (Coronation) and porphyritic (Mara) samples. The porphyritic sample shows dark grains that are likely pyroxene megacrysts in a fine-grained mesostasis containing andesine needles. Both types have magnesium-poor basaltic compositions and in this respect are similar to the evolved Jake Matijevic rock analyzed further along the Curiosity traverse both with Alpha-Particle X-ray Spectrometer and ChemCam instruments. The second rock type encountered is a coarse-grained intrusive rock (Thor Lake) showing equigranular texture with millimeter size crystals of feldspars and Fe-Ti oxides. Such a rock is not unique at Gale as the surrounding coarse gravels (such as Beaulieu) and the conglomerate Link are dominated by feldspathic (andesine-bytownite) clasts. Finally, alkali feldspar compositions associated with a silica polymorph have been analyzed in fractured filling material of Preble rock and in Stark, a putative pumice or an impact melt. These observations document magmatic diversity at Gale and describe the first fragments of feldspar-rich lithologies (possibly an anorthosite) that may be ancient crust transported from the crater rim and now forming float rocks, coarse gravel, or conglomerate clasts.

1. Introduction

[2] The Mars Science Laboratory (MSL) rover Curiosity has 10 scientific instruments and 17 cameras on board. Of these, the Chemistry Camera (ChemCam) instrument, located on the top of the rover mast, is the first laser sent to the surface of another planet. This instrument enables elemental analyses of rocks and soils using laser induced breakdown spectroscopy (LIBS), of targets situated at distances of up to 7 m from the rover [*Maurice et al.*, 2012; *Wiens et al.*, 2012]. Furthermore, ChemCam has a high-resolution remote microimager (RMI) capable of identifying exactly where analyses were performed. In light of its capacity to provide rapid semiquantitative estimates of elemental composition, ChemCam has been used as a decisional and tactical tool for roving, but it also provides quantitative constraints concerning the chemistry of the rocks in the vicinity of the landing site, as discussed in detail in this contribution.

[3] Although the principal focus of the MSL mission is the sedimentary rocks of Mount Sharp [*Grotzinger et al.*, 2012], the rocks encountered over the first 50 Martian solar days (sols) consist of small pebbles of various shapes and

[1]LMCM, UMR-CNRS 7202, MNHN, Paris, France.
[2]CNRS-UMR 7359 GeoRessources, Universite de Lorraine, Nancy, France.
[3]CNRS-UMR 7277 IRAP, Universite de Toulouse, Toulouse, France.
[4]Los Alamos National Laboratory, Los Alamos, New Mexico, USA.
[5]Institute of Meteoritics, University of New Mexico, Albuquerque, New Mexico, USA.
[6]CNRS-UMR 6112, LPG Nantes, Nantes, France.
[7]U.S. Geological Survey, Flagstaff, Arizona, USA.
[8]CNRS-UMR 5275, ISTerre, Universite de Grenoble, Grenoble, France.
[9]Department of Earth Sciences, Brock University, St. Catharines, Ontario, Canada.
[10]Department of Astronomy, Mount Holyoke College, South Hadley, Massachusetts, USA.
[11]Division of Geological and Planetary Sciences, California Institute of Technology, Pasadena, California, USA.
[12]SRC, University of Leicester, Leicester, UK.
[13]Space Science Institute, Boulder, Colorado, USA.

Corresponding author: V. Sautter, Laboratoire de Minéralogie et Cosmochimie du Muséum, CNRS-UMR 7202, MNHN, 61 rue Buffon, FR-75005 Paris, France. (vsautter@mnhn.fr)

sizes, with occasional float rocks and conglomerates [*Williams et al.*, 2013], many of which may originate from regions associated with the crater rim [*Palucis et al.*, 2013]. In light of the late Noachian early Hesperian age of the crater, these samples may shed new light on ancient magmatic crust, providing insight into a critical period of Mars' magmatic history.

[4] The study of Martian magmatism, in particular that in the oldest terrains (Noachian) has benefited enormously from the ever increasing number and quality of global-scale observations from orbiting spacecraft and in situ observations made by landers and/or rovers. Observations of mineralogy at the global scale using orbiting instruments such as the Thermal Emission Spectrometer (TES) on board Mars Global Surveyor, Observatoire pour la Minéralogie, l'Eau, les Glaces et l'Activité (OMEGA) on board Mars Express, or Compact Reconnaissance Imaging Spectrometer for Mars (CRISM) on board Mars Reconnaissance Orbiter suggest that the Noachian crust is predominantly basaltic [*Rogers and Christensen*, 2007], characterized by a two-pyroxene composition enriched in a low-calcium end-member relative to younger igneous provinces [*Mustard et al.*, 2005; *Poulet et al.*, 2009] with or without olivine [*Koeppen and Hamilton*, 2008: *Ody et al.*, 2013]. This includes the Noachian crust impacted by Gale crater or surrounding it. On the other hand, feldspar-rich lavas seem to be restricted in extent [*Christensen et al.*, 2000; *Bandfield et al.*, 2004] and only a few isolated kilometer-size outcrops of anorthosite- rich lithology have been recently reported by CRISM within the central peaks of some craters indicating excavation from depth [*Wray et al.*, 2013; *Poulet and Carter*, 2013] and by the High Resolution Imaging Science Experiment (HiRISE) instrument within the lower walls of Valles Marineris [*Flahaut et al.*, 2012]. Note that as alkali feldspar has few distinctive spectral features in visible near- infrared spectroscopy, observations in this spectral range were not useful to constrain their occurrence.

[5] In addition to space-based exploration of Mars, the shergottite-nakhlite-chassignite group of meteorites (SNC) [*Meyer*, 2011] collectively sample at least six different, yet undetermined localities of the Martian crust [e.g., *Nyquist et al.*, 2001; *Grott et al.*, 2013]. Among the SNCs, the basaltic and picritic shergottites offer an important point of comparison with igneous rocks encountered by Curiosity. The former samples lack evidence of abundant felsic minerals and most of them tend to be pyroxene-rich and feldspar-poor, thus depleted in silicon and aluminum with low total alkali content. This has led to the idea that the mantle source of the SNCs was depleted in Al [e.g., *Longhi et al.*, 1992]. However, a direct comparison with igneous rocks at Gale Crater is not a simple matter given the fact that shergottites are generally considered to be Amazonian in age [*Nyquist et al.*, 2001], although Pb-Pb ages of some shergottites have been interpreted to indicate a Noachian age [*Bouvier et al.*, 2009]. Although the relatively young, low-K SNCs are very well characterized, they may not be typical of older, more voluminous Martian crust seen from orbit by the Gamma Ray Spectrometer and TES [*McSween et al.*, 2009]. The newly found North West Africa (NWA)7034 meteorite is somewhat of an exception, being the first SNC breccia ever described, with a low-calcium pyroxene (LCP) feldspar-rich mineralogy [*Agee et al.*, 2013] with clasts of Noachian age [*Humayun et al.*, 2013].

[6] A third source of data relevant to the magmatic crust of Mars is the in situ investigation by the Mars Exploration Rover

Spirit in Gusev Crater, the most thoroughly studied igneous province on Mars. Thanks to a combination of analytical techniques, olivine-rich basalts (Adirondack class) were found to dominate the floor of this Hesperian age crater [*McSween et al.*, 2006a]. However, Spirit also found evidence for alkali-rich lithologies (e.g., Wishstone, Algonquin, Backstay, Irvine, and Barnhill classes) in the Noachian terrains of the Columbia Hills. These alkali, Al and Ti-rich rocks, that may be related to Adirondack basalts through fractional crystallization [*McSween et al.*, 2006b] or by varying degrees of partial melting [*Schmidt and McCoy*, 2010] do not show visible feldspar clasts [*Squyres et al.*, 2006].

[7] In summary, currently available petrologic insights argue for a Martian crust that is broadly basaltic [*McSween et al.*, 2009], with little evidence for feldspar-rich lithologies. This may be a surprise in light of model compositions of the primitive Martian mantle derived from the geochemistry of the SNCs, as well as global-scale study of the Martian crust using the gamma ray spectrometer on board Mars Odyssey, that both indicate that Mars is enriched in iron and volatile incompatible elements (such as Na and K) relative to the Earth [*Dreibus and Wänke*, 1985; *Taylor et al.*, 2006]. Low degree of partial melting of compositions such as that proposed by *Dreibus and Wänke* [1985] should produce magmatic liquids with concentrations of alkalis and large-ion lithophile elements such as Rb, Sr, Ba, and Li, that are at least as high as those produced on Earth at comparable conditions.

[8] The Noachian-aged rocks around Gale Crater are thus an important additional source of information concerning the diversity of magmatism on early Mars and only the second opportunity (after the Columbia Hills) to potentially study magmatic rocks of this age in situ. In the present paper, LIBS spectra of rocks provided by ChemCam are analyzed in detail for the first time, using statistical tools that allow classification in terms of mineral and rock compositions, made possible by the fact that the ChemCam laser provides analyses at the scale of ~100 µm. In detail, we will focus on the analysis of five float rocks (Coronation, Mara, Thor Lake, Preble, and Stark) and gravels (Beaulieu) encountered at Bradbury Rise.

2. Geological Context: The Bradbury Rise

[9] The MSL rover named Curiosity touched down on the floor of Gale Crater on 6 August 2012 at −4.59, 137.44° in the Bradbury Rise. As seen from orbit (Figure 1a), Bradbury landing site (white cross in Figure 1a) is located in a plain, at a distal portion of the alluvial fan derived from Peace Vallis [*Palucis et al.*, 2013], which transported material from the northern crater rim toward the Bradbury Rise. Over the first 100 sols, Curiosity traveled 500 m to the east (Figure 1b) to Glenelg, which is the contact between three units: (i) the hummocky unit including Bradbury landing site; (ii) an indurated surface with potentially higher crater retention age; and (iii) a lighter-toned fractured unit characterized by high thermal inertia. The hummocky low albedo unit at the Bradbury Rise has abundant gravel (small pebbles of various shapes, sizes, and color; Figures 2a and 2b) with occasional float rocks and conglomerates (Figures 2a and 2c). These conglomerates are composed of grains and pebbles interpreted to be the result of fluvial transport from the crater rim and constitute sediments lying on the bedrock of this region [*Williams et al.*, 2013]. They are comparable to river bed pebbles transported from mountainous regions on Earth.
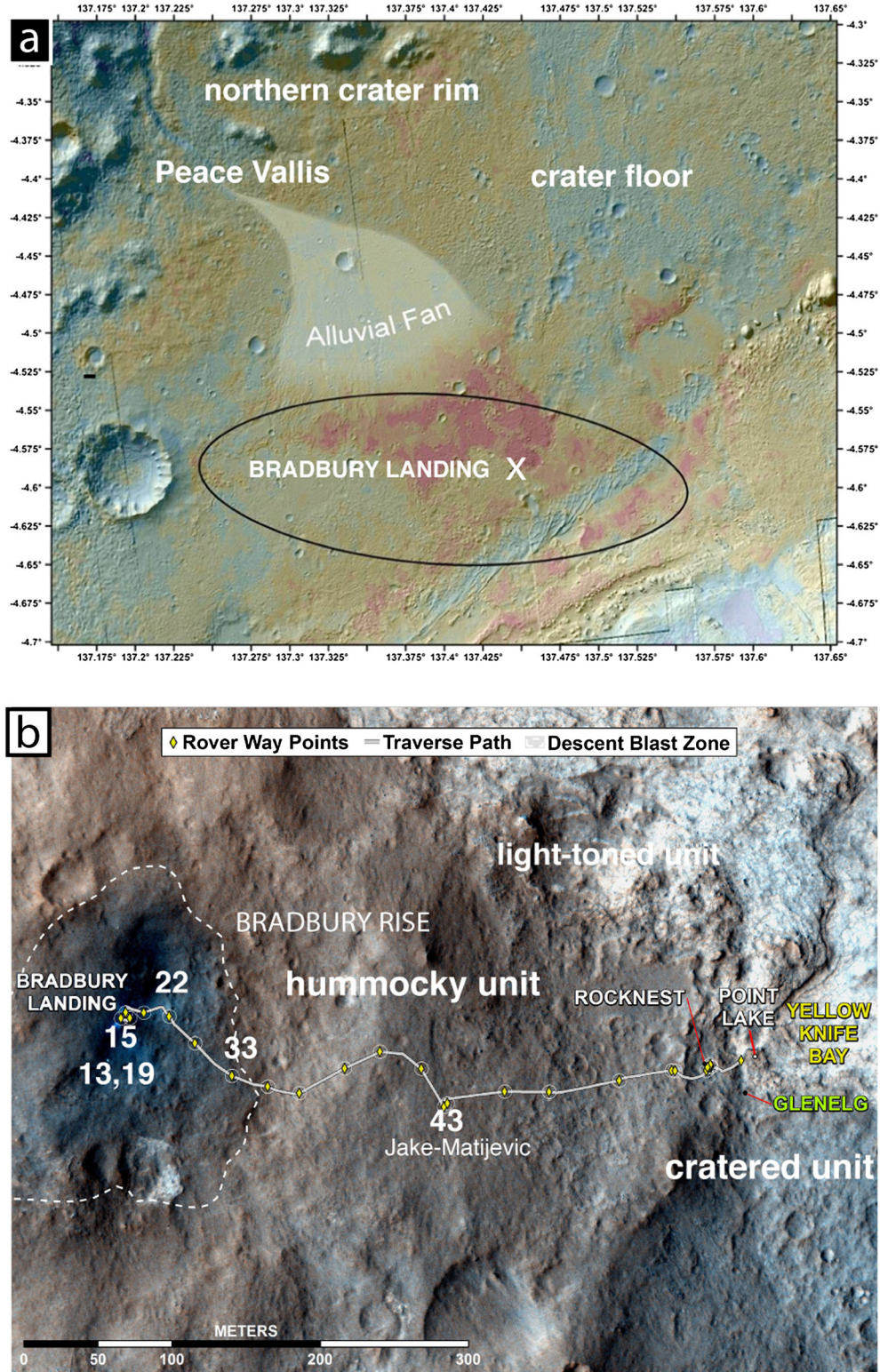
2

Figure 1. Bradbury landing site from orbited Mars Reconnaissance Orbiter images:(a) Peace Vallis within Gale Crater northern rim and its alluvial fan. The landing ellipse, shown in the crater floor, includes a white cross representing the Bradbury landing site; (b) HiRISE image of the Curiosity traverse (white line) from the Bradbury landing site to Glenelg, 500 m to the east. The first 200 m are defined as the hummocky unit. Within this unit, the dark blasted landing site, surrounded by white dashed line, includes the studied samples, localized in their respective sol: Coronation = Sol 13; Stark and Mara0 = Sol 15; Mara1–5 = Sol 19; Thor Lake 1–5 and Preble 1–5 = Sol 22; and Beaulieu 1–5 = Sol 33.
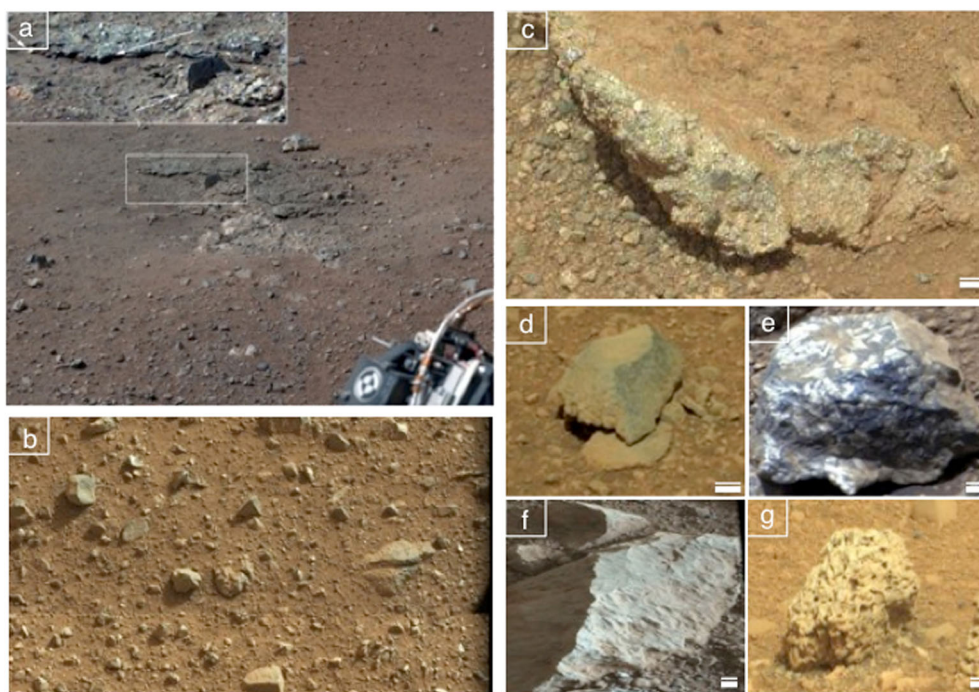
Figure 2. MastCam images of Bradbury landing site showing float rocks overlaying conglomerate bedrock (scale bar is 1 cm): (a) the conglomerate outcrop of Goulburn is shown within the rectangle; (b) float rocks on hummocky terrain; (c) Conglomerate type: Link is composed of clasts including dark, centimeter sized, somewhat rounded gravels and pebbles. From its abundance of rounded material and its proximity to Hottah outcrop, this rock was considered to be part of the same sedimentary unit; (d) Coronation type: dark toned ventifaceted rock such as Mara; (e) porphyritic type: unnamed rock (sol 27) with centimeter-sized light-toned lath-shaped grains; (f) Thor Lake: a ventifacted rock too dusty to be classified; (g) Blanchet type: vesicular light-toned rock with rough texture such as Stark.

[10] The studied area is immediately around the Bradbury site. It is characterized in orbital imagery by darker albedo caused by the descent stage thrusters, which created a blasted area of approximate boundary marked on Figure 1b (dashed white line). Within this zone, most of the rocks are relatively clear of dust, providing unique imaging opportunities. ChemCam targets from sol 13 to 33 are localized in the HiRISE orbital imagery relative to the rover traverse (Figure 1b).

3. Methods and Data Processing

[11] The RMI provides imaging capabilities from 1.2 m to infinity. The field of view (FOV), varies from 4 cm at 2 m to 8 cm at 4 m. It has the highest angular resolution capability of all instruments on board Curiosity with a pixel FOV of 20 μrad. The effective resolution is, however, decreased to 50 μrad due to the dual use of the telescope for both LIBS and imaging. Nonetheless, this angular resolution provides the ability to resolve particles or objects ≈ 100–350 μm in size for standard distances of 2–7 m [*Langevin et al.*, 2013]. During the first 90 sols, the RMI provided excellent context images for LIBS analyses with unambiguous identification of laser spots a few hundred micrometers in diameter, located through comparison of pre-LIBS and post-LIBS images. These imaging capabilities are also complementary to Mast Camera (MastCam) and Navigation Camera for imaging distant rocks and soils at very high resolution. For each observation, two RMI images have been acquired: one before and one after the laser shots. Those images are used to determine grain size and for detailed textural analysis. MastCam data are used for color and overall morphology.

[12] ChemCam LIBS uses a pulsed laser focused on the surface to ablate rocks and soils to create a plasma [*Maurice et al.*, 2012; *Wiens et al.*, 2012]. The size of the laser spot is small and varies with distance, from 350 μm at 1.5 m (distance to the calibration targets positioned on the rover) to 550 μm at 7 m [*Maurice et al.*, 2012]. Each observation point consists of 30 to 50 coaligned laser shots, permitting a study of chemical variations with depth down to 15–30 μm depending on the amount of ablated material. The first few shots remove surface dust and can be used to probe the dust signature. The other spectra are used to trace potential weathering rinds, surface coating, or other chemical changes with depth [*Lanza et al.*, 2013; *Blaney et al.*, 2013]. With such a small beam size, representative sampling of bulk rock composition is restricted to fine-grained rocks (grain size less than 100 μm). When targeting igneous rocks with coarser textures, ChemCam LIBS tends to probe individual grains or binary mixtures rather than the whole rock composition [*Anderson et al.*, 2011; *Cousin et al.*, 2012]. Generally 5 to 9 points measured on each target are sufficient to provide an estimate of bulk composition, provided the targeted rock is not porphyritic [e.g., *McCanta et al.*, 2013].

[13] ChemCam captures the LIBS atomic emission spectrum between 240 and 900 nm from the plasma light from each laser pulse using three spectrometers (UV), visible light spectrometer, and visible to near infrared; *Wiens et al.*, 2012.

Within this range, the LIBS spectrum consists of 6144 channels. Each chemical element is characterized by various emission lines [e.g., *Cremers and Radziemski*, 2006; *Cousin et al.*, 2011]. Typically several hundred emission peaks covering all of the major elements (Si, Al, Fe, Mg, Ca, Na, K, and O) and some minor and trace elements of interest (Li, Cr, Mn, Rb, Sr, Ba, Ti, C, and H) are observed within this range [*Cousin et al.*, 2011]. Several corrections are systematically applied to ChemCam spectra in order to intercompare LIBS spectra from Mars (for noise reduction, continuum and ambient light subtraction, and wavelength calibration) with calibration spectra from Earth (optical transfer function). After these modifications, several methods compete and complement each other to produce composition trends and quantitative compositions.

[14] A number of methods are available for classifying spectra and for qualitative analyses. In the present paper we use Independent Component Analysis (ICA), a multivariate technique that is well-suited to LIBS spectra [*Forni et al.*, 2013a, 2013b]. ICA provides good classification capabilities and allows the assessment of homogeneity within a shot sequence at a single location in order to compare the chemical variability within a series of targets or to test the heterogeneity of a group of neighboring analyses [*Forni et al.*, 2013a, 2013b]. ICA identifies components that are directly related to chemical elements but also mixtures like a "soil" component. This is not a quantitative method per se, but various trends can be highlighted. ICA classification thus opens the possibility to interpret chemical changes in terms of variations in mineral composition.

[15] In addition to the identification of chemical trends, quantification of the abundances of individual chemical elements from the spectral characteristics of the target is of considerable interest. Different approaches can be taken in this respect, for example, univariate analysis or a calibrated version of a multivariate method [e.g., *Wiens et al.*, 2013]. Univariate analysis derives quantitative estimates of composition from the peak height of well-chosen LIBS lines and a training data set to build calibration curves [*Ollila et al.*, 2013; *Fabre et al.*, 2013]. This data set includes the ten onboard ChemCam Calibration Targets (CCCTs) [*Fabre et al.*, 2011a, 2011b, *Vaniman et al.*, 2012]. Multivariate methods are known to give better results in terms of elemental composition, since they incorporate information from the entire spectrum rather than single peaks [e.g., *Clegg et al.*, 2009]. This mitigates the influence of matrix effects and reduces the reliance on any single peak. The PLS1 (Partial Least Squares 1) method is used by the ChemCam team for rapid element determination [*Wiens et al.*, 2013]. This method generates independent models for each of the major elements (SiO_2, TiO_2, Al_2O_3, FeOT, MgO, CaO, Na_2O, and K_2O) by regressing multiple spectra from known calibration standards against the concentration of the element being modeled. Although PLS is capable of generating models that predict multiple major elements at once (PLS2), ChemCam uses PLS1 because it allows the model for each element to be optimized independently. The assumption made by the PLS model is that any unknown spectra will be similar to the spectra used to generate the model. The training set used by the ChemCam team consists of 66 geostandards including basalt, andesite, rhyolite, dolomite, sulfates, olivine, nontronite, kaolinite, dacite, and syenite. The PLS model performs well when the composition of unknown materials falls within the range of compositions spanned by the training set (e.g., fine-grained basalts). PLS performs more poorly when extrapolating beyond the range of training set compositions (e. g., pure minerals). Accuracy of the PLS model is estimated using a leave-one-out cross-validation method. This method iteratively removes one geostandard from the training set, generates a model using the remaining training set standards, and predicts the composition of the sample that is held out. This allows each of the training standards to be treated as an "unknown" and gives a conservative estimate of the accuracy of the model for true unknown samples. The accuracy is summarized by calculating the root-mean-squared error of the cross-validation predictions.

[16] Twenty-three observation points, consisting of 1130 individual LIBS spectra have been acquired on the six studied targets (Coronation, Mara, Thor Lake, Preble, Stark, and Beaulieu). Each of the 23 observations was made with 30 or 50 coaligned laser shots: each shot provides a spectrum at successive depths to 15–20 μm inside the target [*Wiens et al.*, 2012]. The choice was made to first classify each spectrum using ICA to identify the mineral mixture within a given target, compositional variations in a given mineral solid solution, and the presence of nonsilicate phases. The selected components correspond to trends in Ca, Si + Al, K, Na + K, Fe, Si, and Na. Peak heights are checked for qualitative and relative abundance of H, Si, Fe, Mg, Ca, and Ti. Some information from the low-intensity emission lines of the trace elements Ba, Sr, Rb, and Cr is provided by a preliminary study of peak fitting and univariate quantification of these elements [*Ollila et al.*, 2013, this issue]. Once these data have been presented, we illustrate elemental compositions quantified using the simple univariate method obtained from onboard CCCTs. For this quantification the most stable emission lines are selected for calculating the emission areas of the peaks after normalization to the total emission of each spectrum [*Fabre et al.*, 2013]. All selected peaks are fitted with a Lorentzian profile. Independent calibration curves are used to derive specific element ratios, which minimize matrix effects and variations in ablated mass: this is done for Al/Si and (Fe + Mg)/Si. These ratios are commonly used for terrestrial and Martian geological comparisons. Error bars corresponding to statistical variations of the regression lines are estimated to be around 20 relative %. The PLS1 method was also used to quantify composition, but only when that composition was close to basaltic.

4. Rock Morphology and Texture

[17] The float rocks encountered at the Bradbury landing site (Figure 2) are heterogeneous, and grade in color from dark grey to tan and include many faceted rocks. These ventifacts are typical of wind abrasion and are also observed on Earth [*Bourke et al.*, 2007]. From morphology, color, grain size, and patina at least five different groups of rocks have been described [*Yingst et al.*, 2013].

[18] 1. Link-Hottah type (Figure 2c): loose rounded particles like Beaulieu gravels are associated with conglomerate rocks which show cemented equidimensional rounded clasts ranging from 5 to 40 mm in diameter, and showing albedo variations from dark-toned to light-toned. These rocks are
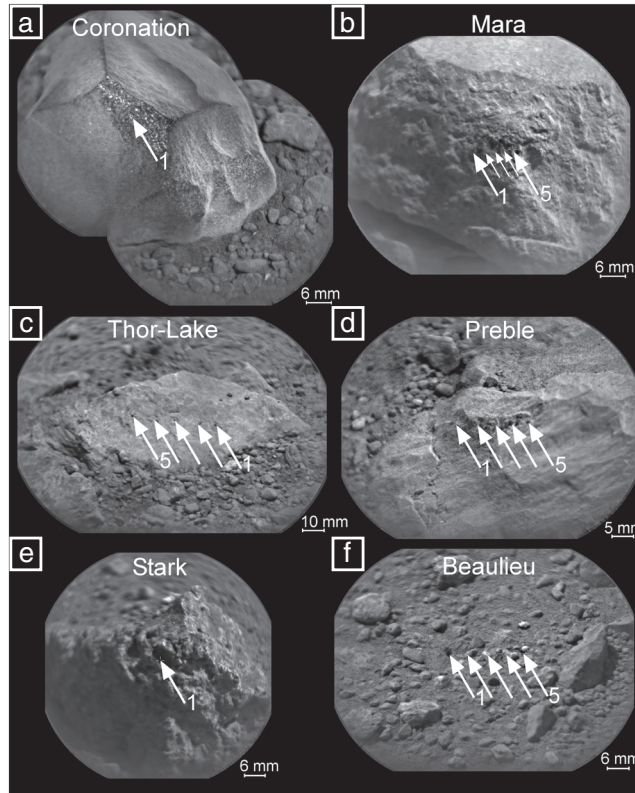
Figure 3. RMI high-resolution images of the six selected targets with the LIBS observations point underlined by a white arrow: (a) Coronation (grain-size less than 0.5 mm); (b) Mara (rough surface due to a coarser texture with dark and white needles-shaped grains up to 1 mm); (c) Thor Lake (light-toned dusty rock); (d) Preble (raster points seem to be aligned along a fractured zone); (e) Stark (pitted surface morphology); (f) Beaulieu (typical soil in hummocky terrain) where ChemCam hit rounded pebbles of 2–4 mm. Note that points 2, 3, and 4 are white pebbles).

interpreted as fluvial conglomerates due to the abundance of rounded pebbles, the presence of imbrication and layering [*Williams et al.*, 2013].

[19] 2. Coronation type (Figure 2d): most rocks have flat or curved facets ending in sharp or rounded edges and are exclusively dark colored. Grain size is variable. Flat facets, keel, flutes, and undulating breakage/wear patterns are common characteristics of basalts fragments.

[20] 3. Porphyritic type (Figure 2e): these differ from any type of rock seen at the other landing sites with light-toned, bladed, and polygonal crystals 1–15 mm in length which look like euhedral plagioclase phenocrysts embedded in a darker, fine-grained, grey matrix.

[21] 4. Wolverine type (Figure 2f): rocks show layering between light-toned and dark-toned material.

[22] 5. Blanchet type (Figure 2g): rocks are mottled and pitted with light tan patina blades. They show voids and pendants and look like pieces of scoria.

[23] With the exception of the Link-Hottah type, these rocks all appear to be clearly of igneous origin, but ChemCam did not analyze all of them. In the present paper we focus on five rocks encountered during the first 100 sols (Figure 3): Coronation, Mara, Thor Lake, Preble, and Stark and gravels (Beaulieu) with the aim of confirming their igneous origin through characterization of their mineralogy and their composition.

[24] Coronation (Figure 3a) has a smooth surface corresponding to fine-grained particles (less than 300 μm). It was targeted on sol 13 at a distance of 2.7 m corresponding to a beam size at the sample of 400 μm; thus, larger than the typical grain size.

[25] Mara (Figure 3b) has a rough surface due to coarse grains, approximately 2–3 mm in size. It seems to be composed of dark anhedral millimeter-sized coarse crystals, fine white needles, and a greyish ground mass. Mara was targeted initially on sol 15 with one observation point at a distance of 4.17 m corresponding to a beam-size at the sample of 450 μm and an RMI image FOV of 9 cm. A second series of analyses was performed on sol 19 (Figure 3b) using a horizontal raster of 5 points in 5 mm intervals and with a beam-size for each point of 400 μm. As the rock seems to be coarse-grained with millimeter-sized minerals 10 times larger than the spot size, single observations can yield the composition of individual grains and grain boundaries.

[26] Thor Lake (Figure 3c) and Preble (Figure 3d) were analyzed on sol 22 with horizontal 1 × 5 rasters at respective distances of 5.32 and 2.68 m and beam sizes of ~500 μm and 400 μm, respectively. Note that the laser pits are detectable on postanalysis RMI images for Thor Lake and Preble while hardly seen on less dusty rocks such as Coronation and Mara.
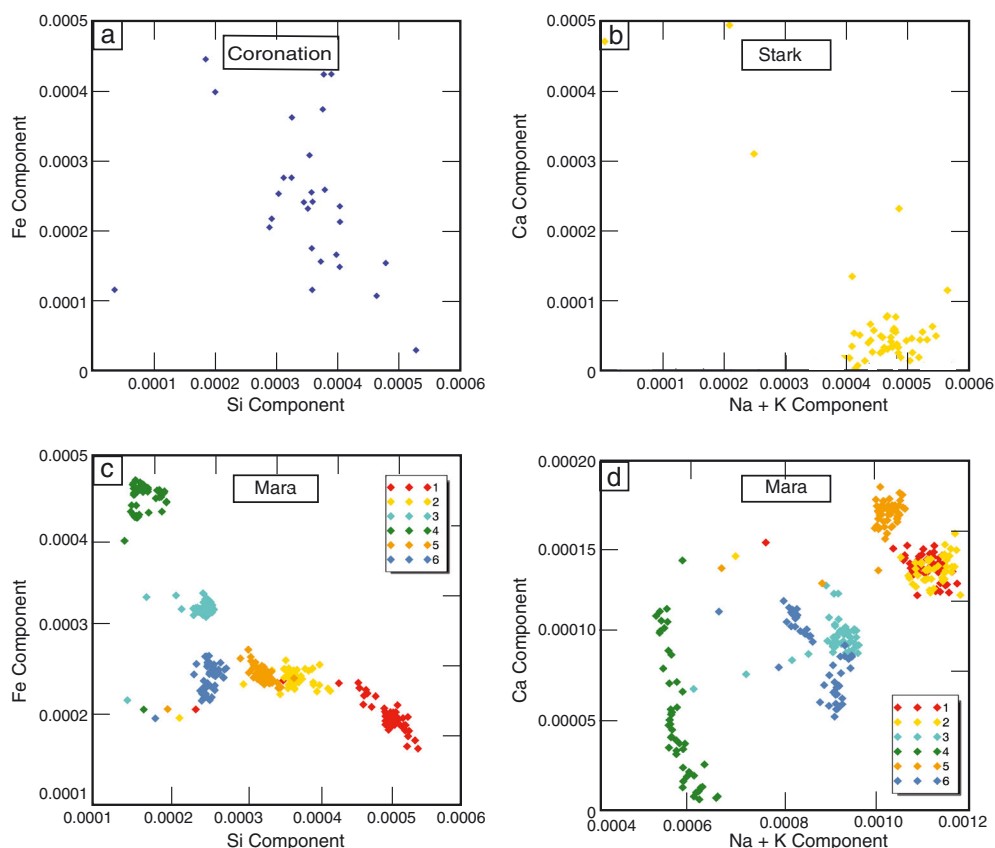
Figure 4. ICA diagram for Coronation, Stark, and Mara. They show shot-to-shot variations in composition with depth between the 30–50 spectra for each of the 23 observation points. The components on the *x* and *y* axes represent a set of independent vectors that define a new basis in which the original spectrum can be plotted. These plots show the correlation coefficient of the represented element in arbitrary units on the *x* and *y* axes. For each color code corresponding to a given observation point within a raster, few (less than 5) isolated points are observed corresponding to the first shots, whilst all the other shots (25 to 35 shots) gather within a given cluster: The former few points represent the dust, the latter 25 or 35 points represent the rock sample in depth below the dusty surface. (a) Coronation: Fe component versus Si. The 30 spectra show variable compositions with respect to these 2 components. (b) Stark: Ca versus Na + K (identical for Na versus Si and Na versus Ca, not shown here). The 45 spectra are close to each other within a single cluster thus pointing to a unique composition, (c and d) Mara in Fe versus Si and Ca versus Na + K. Among the six observation points, Mara 0, 1, and 4 are somewhat similar while, the other points form three distinct clusters. Note the relative dispersion of the spectra within each cluster.

[27] Stark (Figure 3e) is a pumice-like rock with a distinctive whitish color (Figure 2g) analyzed on sol 15 at a distance of 4.74 m, thus with a spot size of 475 μm. Beaulieu gravels (sol 33, Figure 3f) are coarse-grained and are representative of type 2 felsic soils described by *Meslin et al.* [2013]. This target includes three distinct loose pebbles (Beaulieus 2, 3, and 4) with sizes ranging from 3 to 5 mm in diameter. Most of them are white.

[28] The morphology of conglomerate rocks, Link (Figure 2c) and Goulburn (Figure 2a), has been described in companion papers [*Williams et al.*, 2013; *Minitti et al.*, 2013]. Peacock Hill (Wolverine class) [*Yingst et al.*, 2013] has not been included in this study because only one analysis is available while the texture shows clear evidence of compositional layering. Coronation, and possibly Mara belong to the Coronation group (Figure 2d). Stark is from the Blanchet class (Figure 2g). The feldspar-bearing porphyritic group was not sampled during the first 33 sols. If Thor Lake (Figure 2f) and Preble are greyish and ventifacted versions of the Coronation group, they are nonetheless too dusty to be classified properly based on imaging.

5. Mineralogy

[29] There are 23 observation points on the six targets described above (Coronation, Mara, Preble, Thor Lake, Stark, and Beaulieu). The 1130 (30 or 50 coaligned laser shots per point) resulting spectra have been classified in multidimensional component space at different levels: at the observation point level within each target and at target level.

5.1. Depth Profiling

[30] For each rock target, ICA representations (Figures 4 and 5) have been used to classify shot by shot variations in
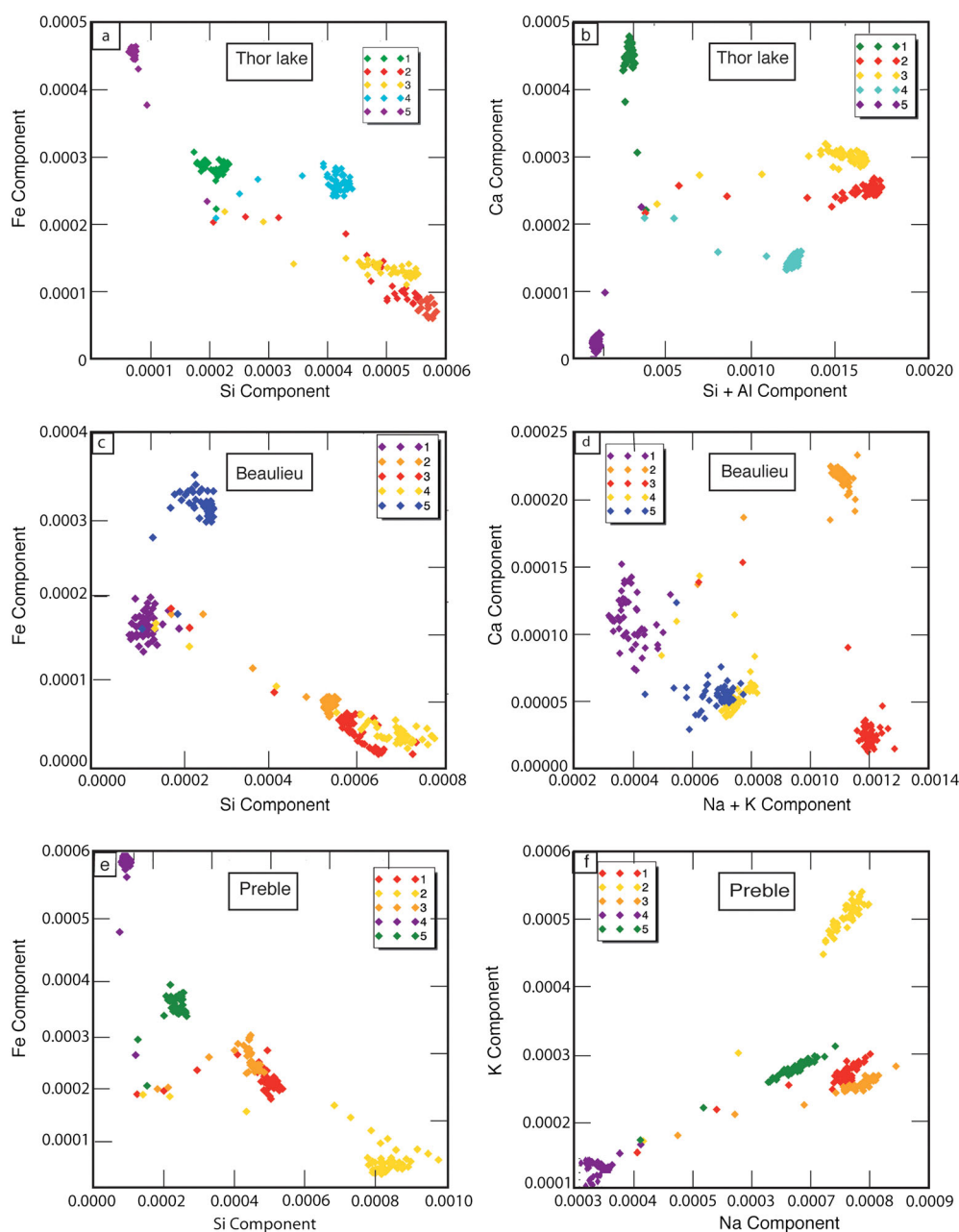
Figure 5. ICA diagram of Thor Lake, Beaulieu, and Preble: (a) Thor Lake in Fe versus Si and (b) Ca versus Si + Al. Thor Lake 1,4, and 5 form three distinct clusters, while Thor Lake 2 and 3 have similar composition; within each cluster, spectra are close to each other. Thor Lake 5 is Fe-rich Ca-poor and plot at a Si value close to zero; conversely, Fe-poor points, Thor Lake 2 and 3, are Si, Al, and Ca-rich. (c) Beaulieu in Fe versus Si and (d) Ca versus Na + K. Beaulieu 2, 3, and 4 clusters are close to each other within the Si–rich side while Beaulieu 1 and 5 plot on the Fe-rich side. Beaulieu 2 is both alkali and Ca-rich, while Beaulieu 3 is Ca-poor but alkali-rich. Within each cluster, spectra are dispersed. (e) Preble Fe versus Si and (f) K versus Na. Preble 1 and 3 are similar while 2 (Si-rich and alkali-rich), 4 (Fe-rich, alkali- and Si-poor), and 5 cluster in different fields.

composition with depth for a given observation point. In such representations, the *x* and *y* axes do not represent absolute concentrations but components that are dominated by the emission line of one single element. For example, the "Si-component" is dominated by the silicon emission lines and what is plotted is the projection of the spectra onto that component. It is consequently proportional to the silica content. For the six analyzed targets and for all observations points, the first few laser shots sample the dust and reveal a common

composition different from the interior of the rock. Excluding these initial laser shots, the observation points are different enough to define distinct clusters for a given rock target when treated with ICA. In this case, each cluster is likely to represent an individual mineral or a mixture thereof if the grain size is smaller than the beam size. For each sample the most variable compositional dimensions (as derived from ICA) will be presented. To aid mineralogical and/or petrological interpretation, the spectral

characteristics of these ICA end-members are used to define the chemical element(s) that is (are) showing variation. Compositional variations may also be observed within a given cluster indicating mineral mixture at micrometric scale or mineral zonation in a given grain.

[31] In Coronation where a single observation was performed (comprising 25 individual dust-free spectra), alkali and Fe, Mg, Ca, and Ti ICA components all show variations. In Figure 4a, we show, for example, in the Fe-Si space that the points are scattered indicating a compositional heterogeneity within the analyzed volume of 15 μm deep × 400 μm diameter. Coronation therefore appears, at least from this one observation point, to be heterogeneous at the laser beam scale, consistent with a grain size (100–200 μm, Figure 3a) smaller than the beam size but not small enough for the individual laser shots to probe a homogeneous mineral mixture (Figure 3a). For the unique observation point of Stark (Figure 4b), the 45 individual laser shots below the dust are close to each other thus indicating a homogenous composition with depth.

[32] For Mara (6 points of 50 shots each), the 270 dust-free spectra define 6 separate clusters in multivariate space for different ICA components (i.e., those associated with Fe versus Si or Ca versus Na + K: Figures 4c and 4d). Mara is thus heterogeneous at the scale of different observation points (separated by 5 mm). Each observation point defines a separate compositional cluster consisting of 45 spectra. These six different compositional end-members are consistent with coarse grain sizes (up to 1 mm for the dark crystals) relative to the beam size. Nevertheless, some variation is seen for a given point, indicating a degree of small-scale chemical heterogeneity corresponding to mineral and or glass mixture at some point. The point Mara 3 (green diamond in Figures 4c and 4d) illustrates this particularly well, with a clear drop in the intensity of the spectral component associated with Ca from shot 10 to shot 50, at constant Na + K suggesting that the laser beam is profiling into a deeper mineral grain whose composition is that of a ferro-magnesian silicate mixed with some feldspathic component.

[33] In Thor Lake (Figures 5a and 5b) five distinct clusters corresponding to the five observation points are observed. Within each cluster, spectra are quite close to each other in various representations (Fe versus Si; Ca versus Si + Al; including Na + K versus Fe and Si + Al versus Fe not represented in Figure 5) except the alkali-rich points (Thor Lake 2 and Thor Lake 3, Figure 5b) that show positive linear correlation of ICA components associated with Ca and (Si + Al) on the one hand, (Figure 5b) and a negative one between those representing Fe and Si on the other hand (Figure 5a). We therefore conclude that the laser has sampled distinct individual phases with either homogeneous composition or showing some degree of chemical-zoning feldspar showing variations in anorthite composition.

[34] Among the gravel points analyzed in the Beaulieu target (Figures 5c and 5d), at least three of them form a distinctive alkali- and Si-rich end-member (Beaulieu 2, 3, and 4) while it is inferred that Beaulieu 5 has a ferro-magnesian composition. All targeted points display some compositional variation with depth.

[35] For Preble (Figures 5e and 5f), the scatter between spectra acquired at the five different points is comparable with the scatter observed in Thor Lake. Some minor shot-to-shot variation is also present, likely due to variations in mineral contribution to each point.

[36] Therefore, except the point analyzed in Coronation (Figure 4a) which shows significant shot-to-shot variation in composition (indicating heterogeneity at the laser beam scale), the other 22 observation points typically define a restricted compositional range, related to the presence of single phases, or binary/ternary mixtures that we will now attempt to constrain.

5.2. Striking Features Within Six Targeted Points

[37] In order to compare the composition of the targeted points, an average LIBS spectrum was calculated at each of the 23 observation points (Figure 6), omitting the first five shots to avoid dust contamination. All targets showed essentially no hydrogen peak (excluding the shots related to the surface dust). The mean LIBS spectrum of Coronation shows many similarities to that of the basalt from our database [*Wiens et al.*, 2013].

[38] All targets include a spectral component characteristic of Si, except two notable points (Thor Lake 5 in Figure 6a, and Preble 4). All targets also show spectral features indicative of the presence of Fe and Mg but with variable intensity. In this respect, Stark has the smallest contribution of Fe-Mg peaks (Figure 6a). Mara, Thor Lake 2 and 3, and Preble 1 and 2 also appear to be relatively poor in Fe and Mg and rich in Si and alkalis (indicative of felsic minerals), when compared to all the other observation points, as discussed in more detail below. Among the spectra rich in Fe-Mg (Figure 6b), Mara 3 displays high-intensity Fe (Mg) peaks with a low contribution Ca components. On the other hand, Thor Lake 1 is higher in calcium and magnesium and shows a notable chromium peak. Overall, Thor Lake 5 and Stark reflect two extreme compositions, the former being rich in Fe and Ti, but poor in Si, while the latter is rich in alkalis and Si but poor in Fe and Mg. Mara 3 and Thor Lake 1 have intermediate spectra that could be dominated by ferro-magnesian silicates. All the other spectra correspond to mixing in various proportions of ferro-magnesian and felsic components requiring further data processing.

5.3. Mineral Classification

[39] Average spectra from each of the 23 analysis points have been investigated with ICA (Figure 7). Figures 7a and 7b show the covariation of the principal components Fe versus Si and Na + K versus Si, respectively, allowing the description of two mixing lines. In Fe versus Si space (Figure 7a), the two components are anticorrelated and a mixing line may be drawn between Fe-rich Si-poor (purple cluster) and Si-rich Fe-poor analyses (orange cluster). In the purple cluster, containing two targets (Thor Lake 5 and Preble 4), the high-Fe component with virtually no silica may correspond to iron oxides. At the other extreme, the Fe-poor Si-rich orange circle includes 10 targets. Interestingly in the Na + K versus Si diagram (Figure 7b), these 10 Si-rich targets are all concentrated in the alkali-rich domain at the upper right hand corner of the diagram. This Si and alkali-rich cluster (shown in orange cluster of Figure 7b) includes 10 points: Thor Lake 2 and 3; Stark; Preble 2 and 1, Mara and Mara 1, Beaulieu 2, 3, and 4. Note the decreases of Na + K /Si ratio from Mara 1 to Stark toward the extreme value of macusanite (blue diamond in Figure 7), a felsic volcanic glass from Peru [*Pichavent et al.*, 1988] with 35% quartz, 38% albite,
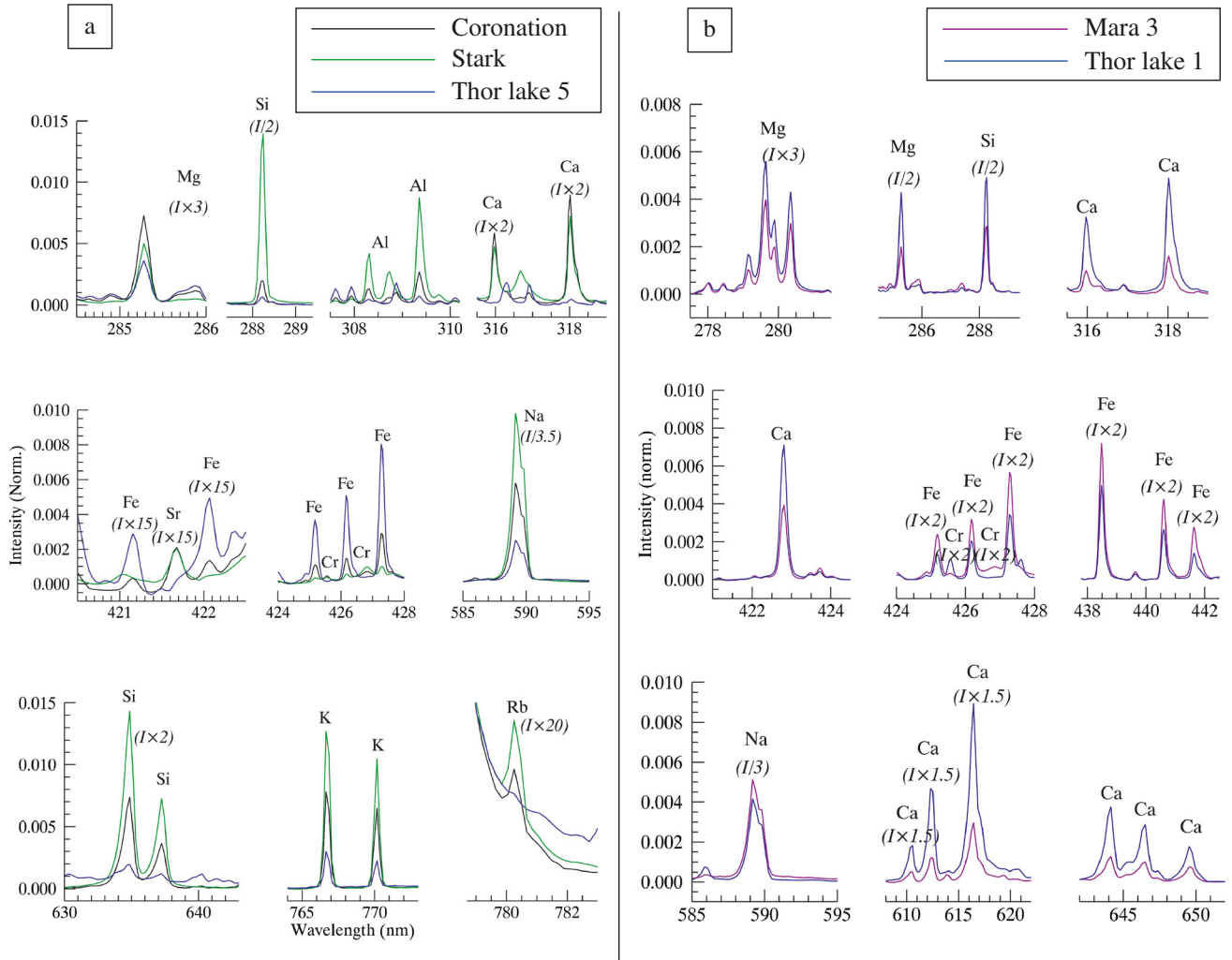
Figure 6. LIBS emission peaks in the ultraviolet (UV) and part of the violet-blue (VIO) and the visible to near infrared (VNIR) spectral ranges. For this figure, the spectra from each analysis point were averaged over depth. Selected individual peaks (Mg, Si, Al, Ca, Fe, Na, K, and Rb) for (a) Coronation, Stark, and Thor Lake 5 and (b) for Mara 3 and Thor Lake 1.

and 23% orthoclase normative composition used as a CCCTs on the rover [e.g., *Fabre et al.*, 2011]. It is then assumed that at least Stark, Preble, and Thor Lake may have felsic composition (feldspars ± silica).

[40] Between Fe-oxides and felsic compositions, other samples broadly define a mixing line although using the Na + K versus Si diagram, three intermediate groups can been distinguished. The low silica, low alkali members of this trend can be assigned to ferromagnesian silicates (Mara 4, Thor Lake 1, and Beaulieu 5). Mixtures of ferromagnesian and felsic material include Coronation, Mara 2 and 5, and Preble 5 and can represent either mechanical mixtures of grain with different compositions or glassy material.

5.3.1. Felsic Component

[41] The largest felsic cluster (orange cluster in Figure 7b) can be subdivided by further ICA analysis, allowing different end-members within the feldspar group to be distinguished: alkali feldspar (albite-orthoclase) and plagioclase (anorthite). In a plot of ICA components associated with (Na + K) and Al (Figure 7c), where aluminum is a proxy for anorthite component, we observe an increase of the anorthite component and

a decrease of the alkali feldspar component in the following order (red dashed line in Figure 7c: Stark, Preble 2, Beaulieu 3–4, Mara, Thor Lake 3, Thor Lake 2, and Beaulieu 2). In a Na versus K diagram (Figure 7d) it is possible to evaluate qualitatively different Na/K ratios. The five observation points of the conglomerate Link studied by *Mangold et al.* [2013], dominated by felsic composition (red ellipse in Figures 7c and 7d), and the macusanite CCCT (blue diamond), have been included in this diagram for comparison. Mara and Mara 1, Thor Lake 2 and 3, Preble 1, and Beaulieu 2–4 are Na-rich, while Beaulieu 3, Preble 2, and three of the Link points plot slightly to the right of a mixing line including macusanite for which Na/K = 0.9, corresponding to the sanidine field (albite ≤ orthoclase).

[42] In conclusion, the ICA approach allows a preliminary classification of the whole set of felsic components observed in Bradbury Rise. Preble points (1, 2, and 3), Beaulieu 3, and Stark plot within albite-orthoclase solid solution: Preble 1–3, Beaulieu 4, and Stark are more albite-rich than Preble 2 and Beaulieu 3. On the other hand, Mara, Thor Lake 2, 3, and 4, and Beaulieu 2 are inferred to be mainly composed of an
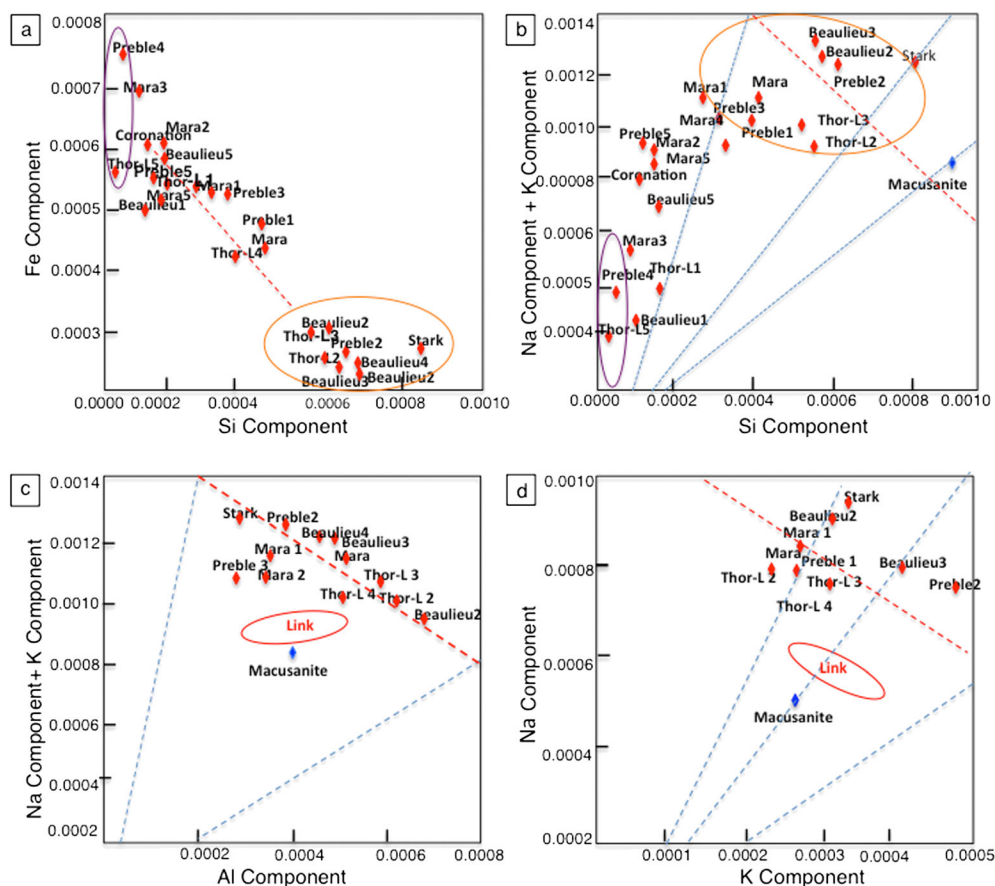
Figure 7. Selected ICA diagram showing the 23 observation points in Mara, Coronation, Thor Lake, Preble, and Stark and the macusanite (blue diamond), a CCCTs on board Curiosity. Plots displaying ICA results show the correlation coefficients of the represented elements in arbitrary units. (a) Fe versus Si shows a negative correlation between two end-members, the Fe-rich Si-poor in purple and the Si-rich and Fe-poor in orange circles. (b) Na + K versus Si diagram shows a positive correlation between the alkali- and Si-poor purple cluster (including the two Fe-rich targets) and the alkali-and Si-rich orange cluster (including the six Fe-poor points of Figure 6a). This orange cluster thus includes all analyzed felsic phases. The red dashed line joins feldspathic and felsic composition with the macusanite at the silica-rich side. (c) Na + K versus Al diagram used for subclassification of feldspar compositions showing variations between albite-orthoclase solid solution (y axes) and plagioclase (x axes); blue dashed lines represent two mixing lines with constant Na + K/Al ratio between felsic and ferromagnesian (toward the origin) end-members; red dashed line shows solid solution between plagioclase feldspars (d) Na versus K diagram shows the relative proportion of albite and orthoclase components within different targets. Three mixing lines with different Na/K ratios are shown in blue dashed lines. Red dashed line joins albite and orthoclase-rich end-members. Red ellipse contains Link data not studied in the present paper.

albite-anorthite solid solution. The Link conglomerate analyses are both anorthite- and orthoclase-rich and may correspond to two feldspar compositions (either a mixture of plagioclase and alkali feldspar or glassy material with felsic composition). This is consistent with the ChemCam analysis of this conglomerate by *Mangold et al.* [2013].

[43] The ICA classification based upon major elements is also supported by trace element data, in particular the presence of Ba and/or Sr and Rb in Mara, Thor Lake, Link, Stark, Preble, and Beaulieu (Table 1) [*Ollila et al.*, 2013], three elements characteristic of feldspars in magmatic systems. In detail the strongest barium peaks have been observed for Preble and Stark with both estimates to have up to 600 ppm. It is well-known that barium, due to its large size, substitutes exclusively with the large potassium cation thus is diagnostic for orthoclase. These points support the ICA classification that attributes Beaulieu 3, Preble 2, and Stark to the albite-orthoclase solid solution. Conversely, Mara, Mara 1, and Thor Lake 2 and 3 are barium-poor but do contain between 290 and 314 ppm of Sr, the atomic size of which is about halfway between those of K, Na, and Ca with the same charge as calcium. This supports the ICA classification identifying these points as plagioclase solid solutions between anorthite and albite. The conglomerate Link is uniquely high in both Sr (≈ 1500 ppm) and Ba (≈ 70–330 ppm), as well as Rb (≈ 200 ppm) reaching concentrations twice as high as other targets encountered in the first 100 sols. These observations are consistent with a mixture of different feldspars sometime associated with silica rather than felsic glasses.

Table 1. Trace Elements Estimations [*Ollila et al.*, 2013]: Abundances Have Been Rounded to the Nearest 10 ppm; "-" Indicate the Abundance Is Not Available [a]

Targets	Ba (ppm)	Rb (ppm)	Sr (ppm)
Coronation	90	340	1550
Stark	550	50	120
Mara	120	30	310
Mara 1	-	30	300
Mara 2	40	20	150
Mara 3	-	-	-
Mara 4	-	40	360
Mara 5	110	30	150
Thor Lake 1	-	-	-
Thor Lake 2	-	30	300
Thor Lake 3	-	30	290
Thor Lake 4	-	30	180
Thor Lake 5	-	-	-
Preble 1	180	40	170
Preble 2	610	70	100
Preble 3	230	30	170
Preble 4	-	-	-
Preble 5	120	40	100
Link 1	100	170	1800
Link 2	70	170	1380
Link 3	330	190	2190
Link 4	140	130	1180
Link 5	300	130	1860
Beechey 2	-	-	290
Murky 2	-	20	440
Murky 4	-	20	300
Beaulieu 2	90	120	520
Beaulieu 3	280	110	510
Beaulieu 4	200	30	270
Kam 7	-	20	350
Kam 9	-	30	260

[a]Ba abundance are from univariate peak area models in *Ollila et al.*, 2013, with a root-mean-square error of prediction (RMSEP) of 640 ppm. Rb abundance are from the partial least squares (PLS) model in *Ollila et al.*, 2013 (error value 30 ppm). Sr abundance are from univariate peak area model in *Ollila et al.*, 2013 (error value 170 ppm).

5.3.2. Oxide Components

[44] Spectra (see section 5.2 and Figure 6) as well as the Fe versus Si ICA diagram (Figures 5a, 5e, and 7a) reveal that two observation points (Thor Lake 5 and Preble 4) are more or less devoid of Si. These spectra also show a prominent titanium peak, suggestive of Fe-Ti oxides (e.g., magnetite-ulvospinel solid solution).

5.3.3. Ferro-Magnesian Silicates

[45] Thor Lake 1 is Cr-rich compared to Mara 3 (630 ppm and 120, respectively [*Fabre et al.*, 2013]. Moreover it is Ca-rich (Figure 5b). Calcium is a trace element in olivine and the presence of Cr is of interest as trivalent cations partition only weakly into olivine while they may partition more freely into pyroxene, through exchange with aluminum in the octahedral cation site. The Ca-rich and Cr-rich component of Thor Lake1 is thus consistent with the presence of a high-calcium pyroxene(HCP) component. Mara 3 is Fe-rich (Figure 4c) Na + K-poor (Figure 4d) but does contain substantial calcium that drops with depth. At that stage it is thus hard to tell whether it represents a mixture of two pyroxenes (HCP and LCP) or orthopyroxene.

5.4. Preliminary Univariate Quantification

[46] In general terms, Al/Si versus (Fe + Mg)/Si diagrams can aid in distinguishing the igneous minerals quartz, feldspar (albite-anorthite solid solution), nepheline, augite (HCP), orthopyroxene (LCP), olivine (fayalite-forsterite solid solution), and Fe-Ti oxides (Figure 8). In this representation, feldspars and feldspathoids are plotted on the *y* axes, while ferro-magnesian minerals are plotted on the *x* axes. Quartz (or other silica polymorphs) are plotted at the origin, while Fe-Ti oxides fall in the upper right corner. Mixtures of pyroxene, olivine, and feldspar typical of basalt may therefore be expected to define a three-phase triangle. Increases or decreases in the abundance of one or more minerals results in compositional trends away from an apex of that triangle. For points within these triangles, it is impossible to distinguish chemically a mechanical mixture of different minerals from glassy material with a basaltic composition. In light of the potential use of the Al/Si versus (Fe + Mg)/Si diagram, these key element ratios have been quantified by the univariate
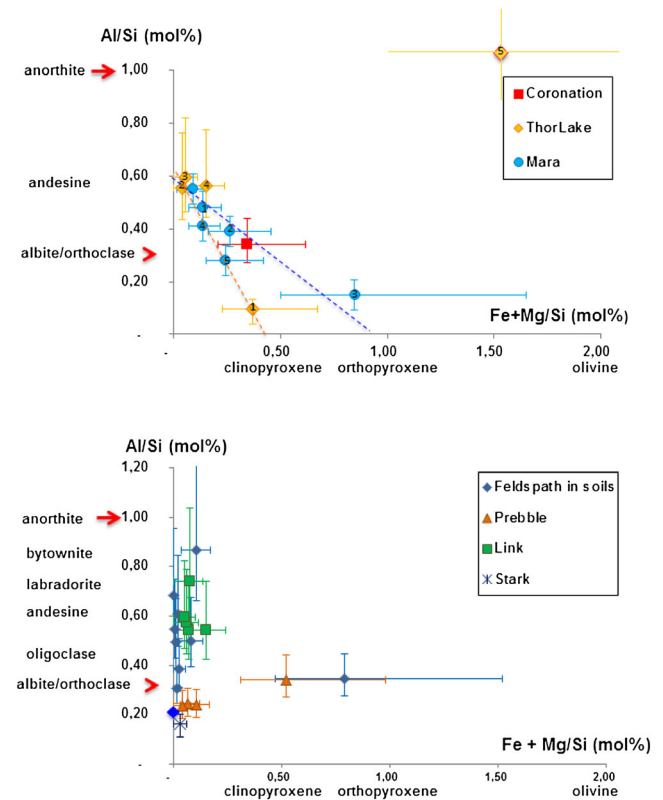

Figure 8. Element ratio diagrams based on element ratios from univariate calibration curves (tabulated in Table 2) for the 23 observations points on the 5 targets and a CCCT macusanite. (a) Igneous mineral and rocks composition plotted in Al/Si versus (Fe + Mg)/Si; Coronation, Thor Lake, and Mara. (b) Felsic-rich composition in Al/Si versus (Fe + Mg)/Si compositional space Stark (black star), Link (green square), Preble (yellow triangle), and different soils (Kam, Beechey, and Murky including Beaulieu, light blue diamonds). The CCCTs macusanite is the dark blue diamond. With the exception of Preble 1 and 4, all observations points plot close to the Al/Si axis corresponding to felsic feldspar-like compositions. In Al/Si versus (Fe + Mg) /Si composition space, the grains range from alkali-rich (albite + orthoclase) feldspar components such as Stark and Preble, and anorthite-rich for some soil grains, with Link showing intermediate compositions.

Table 2. Mole Ratios Obtained Using Peak Emission Ratios From Univariate Calibration Curves [*Fabre et al.*, 2013]

Targets	Al/Si	(Fe + Mg)/Si
Coronation	0.38	0.31
Stark	0.21	0.01
Mara	0.58	0.07
Mara 1	0.52	0.11
Mara 2	0.43	0.23
Mara 3	0.20	0.78
Mara 4	0.45	0.11
Mara 5	0.33	0.22
Thor Lake	0.15	0.33
Thor Lake 2	0.59	0.02
Thor Lake 3	0.63	0.04
Thor Lake 4	0.60	0.13
Thor Lake 5	1.14	1.33
Preble	0.29	0.05
Preble 2	0.29	0.02
Preble 3	0.29	0.08
Preble 4	0.08	1.46
Preble 5	0.38	0.48
Link	0.58	0.05
Link 2	0.61	0.04
Link 3	0.76	0.06
Link 4	0.63	0.03
Link 5	0.58	0.13
Beechey 2	0.89	0.12
Murky 2	0.58	0.02
Murky 4	0.54	0.06
Beaulieu 2	0.64	0.02
Beaulieu 3	0.43	0.07
Beaulieu 4	0.35	0.03
Kam 7	0.71	0.02
Kam 9	0.53	0.10

method described above for each of the 23 depth-averaged selected spectra (Table 2).

[47] The error bars present in Figure 8 have been calculated as statistical variations of regression lines. Thus, the minimum and the maximum variations for each analyzed target are different. Due to the confidence interval of the calibration curve, these variations are the smallest for the compositions that are closest to the standard compositions and higher when the analyzed sample shows greater deviation from the calibration target compositions: this is particularly true for the ferro-magnesian minerals and the oxides. *Fabre et al.* [2013] have observed a difference in the calibration curve between the ceramic and the silicate glass standards, thus explaining the highest relative standard deviation (RSD: around ± 20% for the majority of the 23 observations) for the (Fe + Mg)/Si axes compared to the Al/Si axes in Figure 8.

5.4.1. Mineral Components

[48] Aluminum-rich compositions such as Thor Lake 2, 3, Mara, and Mara 1 in Figure 8a and Beaulieu 2 in Figure 8b have molar Al/Si ranging from 0.5 to 0.6, should correspond to anorthite 34–54% (andesine, Table 3) rather than feldspathoids due to the detection of silica (see Figure 7b). Preble and Stark (Figure 8b) plot close to the macusanite CCCTs at an Al/Si value less than 0.33 (Table 3). Given that pure alkali feldspar (albite and/or orthoclase) has an Al/Si ratio of 0.33, this suggests the presence of silica. Through comparison with the spectrum of the macusanite CCCT, which has a normative composition consisting of 35% quartz, 38% albite, and 23% orthoclase, Preble and Stark should contain a substantial amount of silica. Interestingly, felsic gravels analyzed within type 2 soils of *Meslin et al.* [2013]

(Figure 8b) span a wide range of composition from alkali-rich to aluminum-rich (anorthite end-member).

[49] The two points Thor Lake 5 and Preble 4 plot on the right hand side of the diagram of Figure 8b and appear to correspond to oxide phases. The Thor Lake 5 sample also seems to contain a high Al component; thus, these oxides may be mixed with some alumina–bearing component, i.e., some feldspathic mineral, thus justifying its position in the top left corner of the diagram. Finally, Thor Lake 1 plots closer to the clinopyroxene field of Figure 8a, whilst Mara 3 is close to an orthopyroxene mixed with some aluminum.

5.4.2. Complex Assemblages

[50] The samples considered above represent the principal spectral end-members of our data set, inferred to be near pure minerals. On the other hand, many of the observation points appear to be complex mixtures as discussed in this section. The average for Coronation plots close to the center of the basaltic mixing line between feldspar and pyroxene components. Microtextures shown in Figure 3a provide evidence for a fine granular texture rather than the presence of glassy material. Normative calculations from the derived bulk composition using PLS1 (Table 4) indicate a pyroxene-quartz normative assemblage, though comparisons with Alpha-Particle X-ray Spectrometer (APXS) on other rocks suggest that ChemCam PLS1-derived SiO_2 abundances may be slightly (e.g., 2–3 wt%) overestimated, resulting in a very low quartz content in this rock.

[51] For Mara, the basaltic mixing line in Figure 8a joins Mara 3, the pyroxene-rich point, and Mara (the first point on this rock), intersecting the *y* axes close to the composition representing andesine. This mixing line differs from that involving analyses from Thor Lake. Furthermore, we note that Coronation falls along the Mara pyroxene-andesine mixing line. The four other Mara points cluster toward the center with Mara 2 and Mara 5 being close to Coronation while Mara 1 and 4 are close to the andesine end-member. The former probably corresponds to a ternary basaltic mixture involving plagioclase and two pyroxenes, while the latter may be mostly a two-component mixture dominated by the

Table 3. Alkali Feldspar-Anorthite Relative Proportion Estimated From the Molar Al/Si Ratio of Table 2

Targets	Anorthite	Alkali Feldspar
Stark	0	100
Mara	45	55
Mara 1	34	64
Thor Lake 2	45	55
Thor Lake 3	50	50
Preble 2	0	100
Preble 3	0	100
Link 1	45	55
Link 2	48	52
Link 3	70	30
Link 4	50	50
Link 5	45	55
Beechey 2	54	36
Murky 2	45	55
Murky 4	38	62
Beaulieu 2	54	38
Beaulieu 3	20	80
Beaulieu 4	0	100
Kam 7	64	36
Kam 9	38	62

Table 4. Coronation "Whole Rock" Composition: The Oxide Abundances Were Computed Using Partial Least Square (PLS1) Analysis[a]

ROCK	Coronation	RMSEP
SiO_2	54.3	7.1
TiO_2	1.2	0.55
Al_2O_3	8.7	3.7
FeO	16	4
MgO	2.1	3
CaO	7.9	3.3
Na_2O	3.1	0.7
K_2O	1	0.9
Total	100	
NORM		
Quartz	8.8	
Plagioclase	40.3	
Orthose	7.54	
HCP	26.3	
LCP	15.02	
ilm	1.55	

[a]The estimated Root-Mean-Square Standard Error (RMSEP) is given in the second column.

felsic component. These mineral mixtures could correspond to orthopyroxene phenocrysts (dark megacrysts in Figure 9a) within an aphanitic groundmass defined by andesine (white needles in Figure 9a) and greyish interstitial material that could be glassy or a microcrystalline material smaller than the LIBS beam size.

[52] In Thor Lake, homogenous compositions are sampled for each observation point (cf. Figures 5a, 5b and 9b). The 4 points in Figure 8a plot close to the apex of a mixing line between andesine (Thor Lake 2, 3, and 4) and HCP (Thor Lake 1).

[53] A single point in Preble (Preble 5) has a composition close to Coronation, while the other LIBS points on that rock essentially sampled felsic compositions (Figure 8b). Zooming in the 1 × 5 raster area in the RMI image of this dusty rock (Figure 9c), one can see a fracture filled with whitish material. Thus, observation points on Preble seem to have hit essentially this material except for Preble 5, which corresponds to the surrounding rock material and Preble 4, which is an oxide phase.

[54] For Stark, mineral grains are not generally visible in the RMI image. However, the single point for that target sampled the bulk rather than a coating as Na-K variation with
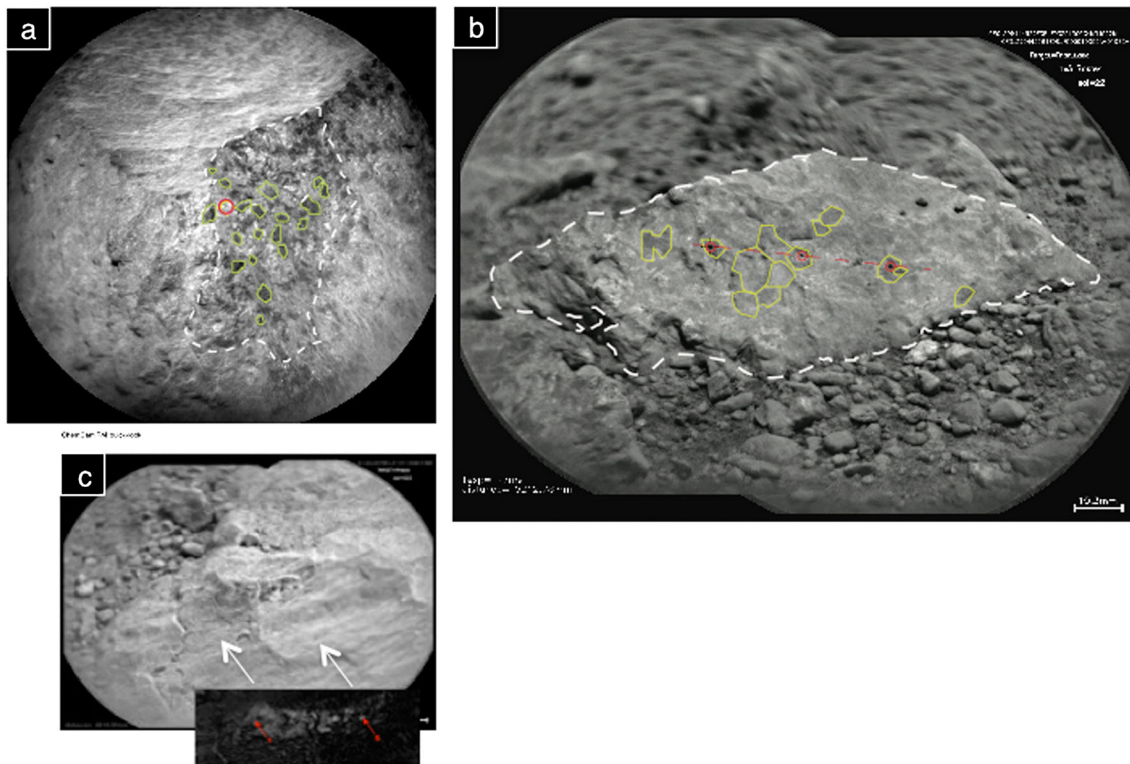

Figure 9. Textural interpretation of Mara, Thor Lake, and Preble rocks shown at the same scale. (a) Dark millimeter-sized Fe-Mg silicate (perhaps LCP and/or olivine, Mara 3) crystals, which appear to be mixed with feldspath (possibly an andesine, white needles in Mara and Mara1) within a greyish fine-grained mineral mixture (Mara 2, 4, and 5). (b) Thor Lake showing a coarse-grained texture of scattered millimeter-sized crystals yielded through that disaggregates the surrounding 5 to 10 mm sized pebbles. ChemCam blind shots hit a majority of feldspar crystals (Thor Lake 2, 3, and 4), one Fe-Ti oxide (Thor Lake 5), and LCP mixed with some andesine component (Thor Lake 1). Note that terrestrial anorthosite dominated by feldspar mineralogy does contain LCP as well as abundant Fe-Ti oxides. (c) Texture of Preble. Between points 1 and 5 is a triangular area containing white patches that look like a fracture filled with light material. This material Stark is an acidic mixture of sanidine and silica phase. The oxide (Preble 4) and the feldspathic-ferromagnesian mixture (Preble 5) may represent minerals from the host rock.

depth is constrained by feldspar mineralogy (Figures 4b and 5a) suggesting that this location is an alkali feldspar (Figure 8b) mixed with silica. As suggested earlier, the RMI and MastCam images (Figures 2g and 3e) indicate that Stark is a pitted rock with a light tan patina showing void and pendants. It could therefore be a piece of scoria or an impact melt with a trachytic kind of composition.

6. Discussion

6.1. Comparison of Coronation and Mara With Jake Matijevic and Rocks From Gusev

[55] As illustrated above, of all the rocks studied by ChemCam over the first 50 sols, only Coronation would appear to have a grain size sufficiently small that the sum of individual spectra within a single observation point on the target is a close approximation to bulk-rock composition. Indeed, on ICA-based diagrams, this rock has an intermediate position relative to feldspathic and mafic components, consistent with a microlithic texture (e.g., grain-size on the order of 200 µm; Figures 3a and 4a). The sample Mara also has few composition points intermediate between feldspathic and ferromagnesian end-members, but in this case some of the grains appear on RMI images (Figure 9a) to be greater in size than the laser beam (grain-size > 500 µm) with millimeter-sized orthopyroxene phenocrysts (see the dark crystal of Figures 3b and 9a) targeted in point 3 within a fine-grained matrix (greyish area in Figures 3b and 9a). Reliable bulk composition estimates would have required at least a 5 × 5 raster for sufficient statistical sampling [*McCanta et al.*, 2013] and thus no attempt to calculate a bulk composition from ChemCam analyses has been made.

[56] We note that the bulk composition derived for Coronation from PLS1 multivariate analysis is with respect FeO-rich, MgO-poor close to that of the rock Jake Matijevic determined by APXS [*Stolper et al.*, 2013]. The sample Jake-M has also been studied by ChemCam, but the grain-size of this rock is well above the size of the laser beam, and there is significant point-to-point variation for this sample [*Cousin et al.*, 2013]. With respect to its Al_2O_3/SiO_2 ratio, Coronation (Table 2) is close to the evolved (low Mg/Fe) alkali-rich rocks of the Wishstone Class observed in the Columbia Hills, as does the Jake Matijevic. On the other hand, despite some chemical similarity, we note that Wishstone Class rocks seem to be pyroclastic [*Squyres et al.*, 2006], while rocks encountered at Bradbury Rise show magmatic textures.

6.2. Comparison of Thor Lake With Beaulieu and Other Gravels at Bradbury Rise

[57] From a textural perspective, Thor Lake was difficult to classify due to its dusty appearance. Chemical data of ChemCam reveal a variability inconsistent with a fine-grained texture (grain size larger than the LIBS spot of 500 µm on that specific target). Closer inspection of RMI in Figure 9b reveals light sinuous lines that could be grain boundaries defining more or less equant coarse grains up to 5 mm across. Thor Lake could correspond to coarse intrusive rock dominated by andesine crystals and containing Fe-Ti oxides or, alternatively, a sedimentary rock such as a strongly cemented pebbly sandstone. In absence of better understanding from the images, we assume an igneous origin as suggested by the chemistry. Textures are

not clear enough to estimate the relative proportion of light-toned versus dark-toned material even though within a raster of randomly selected points, we note that three of five points analyzed were consistent with almost pure feldspar. Interestingly on Figure 9b, the contact between the rock and the surrounding gravels is gradual giving the impression that the latter are the degradation products of the former. Chemically, the coarse gravels such as Beaulieu 2 (Table 3: labradorite approximately An_{55}) studied in the present paper and other felsic coarse granular soils such as Kam, Murky, and Beechey in Bradbury rise [type 2 soils in *Meslin et al.*, 2013] are dominated by plagioclase feldspar with univariate-derived molar Al/Si ranging from 0.5 to 0.9 (Table 2), pointing to an anorthite-rich component (Figure 8b), although PLS1-derived ratios are lower. Furthermore, we note that these coarse-grained soils dominated by felsic mineralogy are in chemical contrast to the average soil component analyzed later on in the traverse at the Rocknest site, the latter of which are similar to soils analyzed elsewhere on Mars [*Meslin et al.*, 2013]. We also note that gravels at Bradbury Rise seem to be composed of lithic fragments of local origin thus suggesting widespread occurrence of a feldspathic (anorthite-rich) mineralogy. These gravels may thus originate from coarse-grained feldspar-bearing intrusive rocks that have become mechanically weathered contributing to the formation of pebbles and the local soil. Thor Lake is the first direct observation at the Martian surface of an intrusive rock containing feldspathic material in abundance. Interestingly, the Martian meteorite NWA 7034 is the first breccia from Mars of Noachian age [*Humayun et al.*, 2013] containing clasts of coarse feldspar and LCP crystals and a bulk composition within the upper range of the basalt field on a total alkali silica diagram [*Agee et al.*, 2013], arguing also for the occurrence of such rock types on Mars.

6.3. Insights Into Noachian/Early Hesperian Magmatism

[58] The abundance of feldspar is also generally low in the Martian rocks studied to date. The ChemCam analyses depict a rather different picture than that indicated by the rocks of Gusev crater and the SNC meteorites. First of all, feldspar appears to be a principal mineral in almost all of the rocks studied, and ChemCam provides the first in situ evidence of coarse-grained (possibly intrusive) magmatic rocks at the surface of Mars containing feldspathic material in abundance. Indeed, study of the Beaulieu gravels and Thor Lake may even suggest the existence of igneous rocks largely dominated by plagioclase (such as an anorthosite). By comparison, the crystalline component of the Mars soil analyzed by the chemical and mineral analyzer instrument was found to contain more than 40% plagioclase [*Blake et al.*, 2013]. It is of interest to note that the principal minerals associated with plagioclase in Beaulieu and Thor Lake are Fe-Ti oxides, a mineral commonly associated with terrestrial anorthosites or related evolved jotunitic liquids [e.g., *Ashwal* [1993]; *Vander Auwera et al.*, 1998]. When combined with the recent discovery of the Martian meteorite NWA 7034 which contains clasts of coarse feldspar and pyroxene crystals [*Agee et al.*, 2013], and the alkali-rich rock Jake Matijevic described by APXS analysis in Gale [*Stolper et al.*, 2013], there is now important new petrologic evidence in favor of the existence of alkali-, feldspar-rich lithologies in at least some regions of the surface of Mars.

[59] Second, major- and trace element evidence (i.e., Ba and Rb) clearly point to the existence of feldspars with a significant K-rich orthoclase component. This result provides further evidence for the existence of alkali-rich parent magmas, but also argues for the possibility of significant differentiation of primary mantle-derived magma before emplacement at the surface, to reach the low Mg# observed and saturation in alkali-feldspar. This latter situation, although common on Earth, appears to be surprisingly rare on Mars, where olivine compositions have been used to argue that primary magmas are not uncommon [e.g., McSween *et al.*, 2006a; *Baratoux et al.*, 2011].

[60] Finally, the possible existence of plagioclase-rich rocks in the vicinity of Gale Crater raises the question of whether a very primitive magma-ocean-related anorthositic flotation crust may have existed on Mars, in a similar way to that suggested for the Moon. However, it is probably too early to speculate on this possibility based upon the data currently available, although further analysis of other float rocks in Gale and assessment of the spatial extent of the source region of these rocks using orbital spectrometers would provide critical constraints on this hypothesis.

[61] Overall, the in situ data from Gale provide unprecedented insights into the diversity of igneous rocks at the surface of Mars, although much more clearly remains to be learned before a complete understanding of Martian magmatism and its variation over time at different spatial scales is available. From these initial MSL data, it appears likely that both subalkaline and alkaline feldspar-bearing rocks are present as ejecta and alluvial fan detritus in the Gale landing site, potentially representative of primitive material from the region surrounding Gale. These felsic compositions should be confirmed by encountering other float rocks in Gale, but the extent of the source region of these rocks will have to be determined from orbit and eventual connection with Medusae Fossae Formation materials to be tested [*Harrison et al.*, 2010]. Characterizing the compositions of igneous source rocks in the vicinity of Gale Crater is also critical to understanding the chemistry of sedimentary materials along Curiosity's path.

References

Agee, C. B., et al. (2013), Unique meteorite from early Amazonian Mars: Water-rich basaltic breccias Northwest Africa 7034, *Science*, doi:10.1126/science.1228858.

Anderson, R. B., R. V. Morris, S. M. Clegg, J. F. Bell, R. C. Wiens, S. D. Humphries, S. A. Metzman, T. Graff, and R. McInroy (2011), The influence of multivariate analysis methods and target grain size on the accuracy of remote quantitative chemical analysis of rocks using laser induced breakdown spectroscopy (2012), Clustering and training set selection methods for improving the accuracy of quantitative laser induced breakdown spectroscopy, *Spectrochim. Acta. B*, 70, 24–32, doi:10.1016/j.sab.2012.04.004.

Ashwal, L. D. (1993), *Anorthosites*, Springer-Verlag, New York.

Bandfield, J. L., V. E. Hamilton, P. R. Christensen, and H. Y. McSween Jr. (2004), Identification of quartzofeldspathic materials on Mars, *J. Geophys. Res. 109*, E10009, doi:10.1029/2004JE002290(2004).

Baratoux, D., M. J. Toplis, M. Monnereau, and O. Gasnault (2011), Thermal history of Mars inferred from orbital geochemistry of volcanic provinces, *Nature*, 472, 338–341, doi:10.1038/nature09903.

Blake, D. F., et al. (2013), Curiosity at Gale crater: Characterization and analysis of the Rocknest sand shadow, *Science*, 341, 1–7, doi:10.1126/science.1239505.

Blaney, D. L., R. Anderson, G. Berger, J. C. Bridges, and N. T. Bridges (2013), Assessment of potential rock coatings at Rocknest, Gale Crater with ChemCam, paper presented at Lunar Planet. Sci. XLIV, Houston.

Bourke, M. C., J. A. Brearlay, R. Haas, and H. Viles (2007), in *A Petrographic Atlas Rock Breakdown Features in Geomorphic Environments*, edited by M. Bourkes and H. Viles, Planetary Science Institute, Tucson, Arizona, USA.

Bouvier, A. J., J. Blichert-Toft, and F. Albarède (2009), Martian meteorite chronology and the evolution of the interior of Mars, *Earth Planet. Sci. Lett.*, 280, 285–295.

Christensen, P. R., J. L. Bandfield, M. D. Smith, V. E. Hamilton, and R. N. Clark (2000), Identification of a basaltic component on the Martian surface from Thermal Emission Spectrometer data, *J. Geophys. Res.*, 105(E4), 9609–9621, doi:10.1029/1999JE001127.

Clegg, S., E. Sklute, M. D. Dyar, J. E. Barefield, and R. C. Wiens (2009), Multivariate analysis of remote laser-induced breakdown spectroscopy spectra using partial least squares, principal component analysis, and related techniques, *Spectrochim. Acta, Part B*, 64, 79–88.

Cousin, A., O. Forni, S. Maurice, O. Gasnault, C. Fabre, V. Sautter, J. Mazoyer, and R. Wiens (2011), Laser induced breakdown spectroscopy (LIBS) library under Martian environment, *Spectrochim. Acta, Part B*, 66, 805–814.

Cousin, A., V. Sautter, C. Fabre, S. Maurice, and R. C. Wiens (2012), Textural and modal analyses of picritic basalts with ChemCam laser-induced breakdown spectroscopy, *J. Geophys. Res.*, 117, E10002, doi:10.1029/2012JE004132.

Cousin, A., et al. (2013), ChemCam analysis of Jake Matijevic, Gale Crater. Paper presented at Lunar Planet.SCi.XLIV, Houston.

Cremers, D. A., and L. J. Radziemski (2006), in *Laser Induced Breakdown Spectroscopy (LIBS) Fundamental and Applications*, edited by A. J. W. Miziolek, V. Palleschi, and I. Schechter, Cambridge Univ. Press, Cambridge.

Dreibus, G., and H. Wänke (1985), Mars, a volatile-rich planet, *Meteoritics*, 20, 367–381.

Fabre, C., S. Maurice, A. Cousin, R. C. Wiens, O. Forni, V. Sautter, and D. Guillaume (2011), Onboard calibration igneous targets for the MSL/ChemCam LIBS instrument, *Spectrochim. Acta B*, 66, 280–289, doi:10.1016/j.sab.2011.03.012.

Fabre, C., et al. (2013), From univariate analyses of the onboard ChemCam calibration targets to estimates of Martian rock and soil compositions, paper presented at Lunar Planet. Sci. XLIV, Houston.

Flahaut, J., C. Quentin, H. Clenet, P. Allemand, J. F. Mustard, and P. Thomas (2012), Pristine Noachian crust and key geologic transitions in the lower walls of Valles Marineris: Insights into early igneous processes on Mars, *Icarus*, 221, 420–435.

Forni, O., S. Maurice, O. Gasnault, R. C. Wiens, A. Cousin, S. M. Clegg, J.-B. Sirven, and J. Lasue (2013a), Independent component analysis classification of laser induced breakdown spectroscopy spectra, *Spectrochim. Acta, Part B*, 86, 31–41.

Forni, O., et al. (2013b), Chemical variability and trends in ChemCam Mars observations in the first 90 sols using independent component analysis (ICA), paper presented at Lunar Planet. Sci. XLIV, Houston.

Grott, M., et al. (2013), Long-term evolution of the Martian crust-mantle system, *Space Sci. Rev.*, 174, 49–111, doi:10.1007/s11214-9948-3.

Grotzinger, J. P., et al. (2012), Mars Science Laboratory mission and science investigation, *Space Sci. Rev.*, 170, 5–56, doi:10.1007/s11214-012-9892-2.

Harrison, S. K., M. R. Balme, A. Hagermann, J. B. Murray, and J.-P. Muller (2010), Mapping Medusae Fossae Formation materials in the southern highlands of Mars, *Icarus*, 209, 2, doi:10.1016/j.icarus.2010.04.016.

Humayun, M., et al. (2013), The age and composition of the Martian Crust from NWA 7533 [#5198 MetSoc 2013].

Koeppen, W. C., and V. E. Hamilton (2008), Global distribution, composition, and abundance of olivine on the surface of Mars from thermal infrared data, *J. Geophys. Res.*, 113(E12), E05001, doi:10.1029/2007JEO2984.

Langevin, Y., B. Gondet, S. Le Mouélic, O. Gasnault, K. Herkenhoff, D. Blaney, S. Maurice, R. Wiens, and the MSL Science Team (2013), Processing approaches for optimal science exploitation of the Chemcam Remote Microscopic Imager (RMI) during the first 90 days of Curiosity operations, paper presented at Lunar Planet. Sci. XLIV, Houston.

Lanza, N. L., et al. (2013), Evidence for rock surface alteration with ChemCam from Curiosity's first 90 sols, paper presented at Lunar Planet. Sci. XLIV, Houston.

Longhi, J., E. Knittle, J. R. Holloway, and H. Wänke (1992), The bulk composition, mineralogy and internal structure of Mars, in *Mars*, edited by H. H. Kieffer et al., pp. 84–208, Univ. Arizona Press, Tucson.

Mangold, N., et al. (2013), ChemCam analysis of conglomerates at Bradbury site, Mars, paper presented at Lunar Planet. Sci. XLIV, Houston.

Maurice, S., et al. (2012), The ChemCam instruments on the Mars Science Laboratory (MSL) Rover: Science objectives and Mast unit, *Space Sci. Rev.*, *170*, 95–166, doi:10.1007/s11214-012-9912-2.

McCanta, M. C., P. A. Dobosh, M. D. Dyar, and H. E. Newsom (2013), Testing the veracity of LIBS analyses on Mars using the LIBSIM program, *Planet. Space Sci.*, *81*, 38–54.

McSween, H. Y., et al. (2006a), Characterization and petrologic interpretation of olivine-rich basalts at Gusev Crater, Mars, *J. Geophys. Res.*, *11*, E02S10, doi:10.1029/2005JE002477.

McSween, H. Y., et al. (2006b), Alkaline volcanic rocks from the Columbia Hills, Gusev Crater, Mars, *J. Geophys. Res.*, *111*, E09S91, doi:10.1029/2006JE002698.

McSween, H. Y., G. F. Taylor, and M. B. Wyatt (2009), Elemental composition of the Martian crust, *Science*, *324*, 736, doi:10.1126/science/1165871.

Meslin, P.-Y., et al. (2013), Soil diversity and hydration as observed by ChemCam at Gale Crater, Mars, *Science*, *341*, doi:10.1126/science.1238670.

Meyer, C. (2011), The Mars Meteorite Compendium, astromaterials res. And Explor. Sci., Lyndon B. Johnson Space Cent., Houston, Tex. [Available at http://curator.jsc.nasa.gov/antmet/mmc/index.cfm].

Minitti, M. E., et al. (2013), MAHLI (Mars Hand Lens Imager) at the Rocknest sand shadow: Science and science-enabling activities, *J. Geophys. Res. Planets*, *118*, 1–23, doi:10.1002/2013JE004426.

Mustard, J. F., F. Poulet, A. Gendrin, J.-P. Bibring, Y. Langevin, B. Gondet, N. Mangold, G. Bellucci, and F. Altieri (2005), Olivine and pyroxene diversity in the crust of Mars, *Science*, *307*(5715), 1594–1597, doi:10.1126/science.1109098.

Nyquist, L. E. D., D. D. Bogard, C.-Y. Shih, A. Greshake, D. Stöffler, and O. Eugster (2001), Ages and geologic histories of Martian meteorites, *Space Sci. Rev.*, *96*, 105–164, doi:10.1023/A:1011993105172.

Ody, A., F. Poulet, J.-P. Bibring, D. Loizeau, J. Carter, B. Gondet, and Y. Langevin (2013), Global investigation of olivine on Mars: Insights into crust and mantle composition, *J. Geophys. Res. Planets*, *118*, 234–262, doi:10.1029/2012JE004149.

Ollila, A. M., H. E. Newsom, R. C. Wiens, J. Lasue, and S. M. Clegg (2013), Early results from Gale Crater on ChemCam detections of carbon, lithium, and rubidium, paper presented at Lunar Planet. Sci. XLIV, Houston.

Palucis, M. C., et al. (2013), Origin and evolution of the Peace Vallis fan system that drains into the Curiosity landing area, Gale Crater, paper presented at Lunar Planet. Sci. XLIV, Houston.

Pichavent, M., D. J. Kontak, L. Brique, J. V. Herrare, and A. H. Clark (1988), The Miocene-Plioce, Macusani volcanics, SE Peru, *Contribution Mineral. Petrol*, *100*, 325–338.

Poulet, F., and J. Carter (2013), Identification of a new rock type on Mars: Anorthosite, paper presented at Lunar Planet. Sci. XLIV, Houston.

Poulet, F., et al. (2009), Quantitative compositional analysis of Martian mafic regions using the MEx/OMEGA reflectance data. 2 Petrological implications, *Icarus*, *201*, 84–101.

Rogers, A., and P. Christensen (2007), Surface mineralogy of Martian low-albedo regions from MGS-TES data: Implications for upper crustal evolution and surface alteration, *J. Geophys. Res.*, *112*, E01003, doi:10.1029/2006JE002727.

Schmidt, M. E., and T. J. McCoy (2010), The Evolution of a heterogeneous Martian mantle: Clues from K, P, Ti, Cr, and Ni variations in Gusev basalts and shergottite meteorites, *Earth Planet. Sci. Lett.*, *296*, 67–77.

Squyres, S. W., et al. (2006), Rocks of the Columbia Hills, *J. Geophys. Res.*, *111*, E02S11, doi:10.1029/2005JE002562.

Stolper, E., et al. (2013), The petrochemistry of Jake Matijevic: A Martian Mugearite, *Science*, *341*, doi:10.1126/science.1239463.

Taylor, G. J., et al. (2006), Bulk composition and early differentiation of Mars, *J. Geophys. Res.*, *111*, E03S10, doi:10.1029/2005JE002645.

Vander Auwera, J., J. Longhi, and J. C. Duchesne (1998), A liquid line of descent of Jotunite (hypersthene monzodiorite) suite, *J. Petrol.*, *39*, 439–468, doi:10.1093//petrology/39.3.439.

Vaniman, D., M. D. Dyar, R. Wiens, A. Ollila, N. Lanza, J. Lasue, S. M. Rhodes, S. Clegg, and H. Newsom (2012), Ceramic ChemCam Calibration Targets on Mars Science Laboratory, *Space Sci. Rev.*, *170*, doi:10.1007/s11214-012-9886-0.

Wiens, R. C., et al. (2012), The ChemCam instruments on the Mars Science Laboratory (MSL) Rover: Body unit and combined system performance, *Space Sci. Rev.*, *170*, 167–227, doi:10.1007/S11214-012-9902-4.

Wiens, R. C., et al. (2013), Pre-flight calibration and initial data processing for the ChemCam laser-induced breakdown spectroscopy (LIBS) instrument on the Mars Science Laboratory rover, *Spectrochim. Acta, Part B*, *82*, 1–27, doi:10.1016/j.sab.2013.02.003.

Williams, R. M. E., et al. (2013), Martian fluvial conglomerates at Gale Crater, *Science*, *340*(6136), 1068–1072, doi:10.1126/science.1237317.

Wray, J. J., S. T. Hansen, J. Dufek, G. A. Swayze, S. L. Murchie, F. P. Seelos, J. R. Skok, R. P. Irwin III, and M. S. Ghiorso (2013), Prolonged magmatic activity on Mars inferred from the detection of felsic rocks, *Nat. Geosci.*, *6*, 1013–1017, doi:10.1038/ngeo1994.

Yingst, R. A., et al. (2013), Characteristic of pebble and cobble-sized clasts along the Curiosity rover traverse from Sol 0 to 90, paper presented at Lunar Planet. Sci. XLIV, Houston.